Linear Time-Variant Chipless RFID Sensor

Nicolas Barbot, Etienne Perret

Linear Time-Variant Chipless RFID Sensor

Nicolas Barbot, *Member, IEEE,* and Etienne Perret, *Senior Member, IEEE*

***Abstract*—In this paper, we present the first chipless sensor which does not satisfy the definition of a linear time-invariant system. This rotational sensor is able to break the time-invariance classically associated with chipless technology by modulating the reflected power in the time domain. As a result, this sensor is able to backscatter power at a frequency different to the one used by the reader and function of the rotational speed. A new identification scheme based on the power of the modulated backscattered tag signal is also introduced and allows to identify different tags. Coding capacity has been evaluated at 11 bits with a probability of correct detection of 98%. Linear time-variant systems allow also to simplify the reader architecture, read multiple tags and increase the read range for both sensing and identification. We show that the proposed chipless sensor could be read at a distance higher than 10 m. This result outperforms classical read range of chipless tag by a factor of 30.**

***Index Terms*—Linear time-invariant system, radar cross section, RFID, scatterer, sensor.**

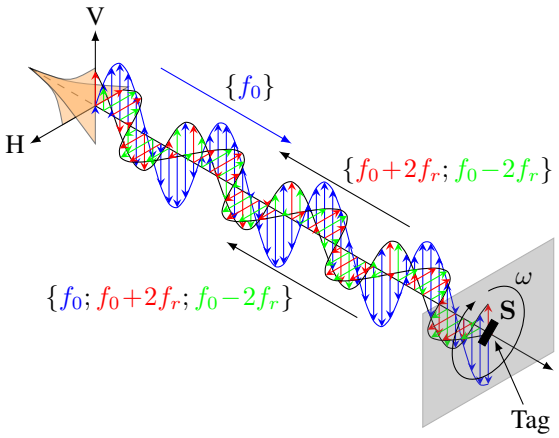

Fig. 1. Principle of the measurement of the proposed method using a dual-access, dual-polarization antenna.

I. Introduction

CHIPLESS technology allows to drastically reduce identification cost compared to classical RFID since the tag does not include any silicon chip. As such, a Chipless Tag (CT) does not contain any memory, any power harverster, and any load modulator. Frequency coded tags are based of resonant structures impinged by a Ultra-Wideband (UWB) signal. When excited by a UWB signal, these structures induce a current at given frequencies and backscatter a power which can be detected by the reader. Since the development of this technology [1], a lot of efforts has been placed to increase the coding capacity [2], the robustness of the reading [3], [4] or to satisfy regulation constrains [5]. However, since a CT is only composed of classical materials (*i.e.*, dielectric and metallic components), the tag itself is a Linear Time-Invariant (LTI) system which is the main difference compared to classical RFID or other telecommunication systems [6]. The linearity impact has mainly been underestimated for the performance study of this technology and has not been covered by the literature.

This paper introduces the first sensor based on the chipless technology which is able to break the intrinsic time-invariance associated to this technology. As such, this sensor can not be considered as a LTI system and can produce frequency components at a different location of the ones sent by the reader. As we will show, this allows to increase the read range of the tag by a factor higher than 30 while simplifying the reader architecture. The proposed concept relies on a Linear Time-Variant (LTV) system (*i.e.*, by modifying the tag response during the interrogation done by the reader). Analytical model is also provided to clearly describe and predict the tag response for any scatterers. The study presented in the paper is based on rotating tags but different movements can be addressed as well (*e.g.*, translation). The operating principle is presented in Fig. 1 where a reader and the rotating tag can be seen. The antenna is aligned with the axis of rotation of the tag. Rotational speed is assumed to be constant. The proposed solution permits to realize both sensing and identification of the tag by using a simple Continuous Wave (CW) reader at a distance higher than 10 m.

Breaking the time-invariance property has already been investigated in the literature [7]–[12]. In [7], authors have placed a CT on a rotating support and measure the envelope of the backscattered signal. Tag is read using a modulated AWGN signal around 915 MHz at a distance of 15 cm. In [8]–[10], authors have reported a 40 bits or/and 160 bits CT(s) composed of multiples identical resonators and use the movement of the tag to read each resonators sequentially. Note that, since the information is encoded spatially, all the resonators can use the same frequency. Also, reading is realized with a simple CW and an envelope detector. More importantly, since variation of the transmission coefficient is achieved by direct coupling between a transmission line and the resonators, the read range of this system is limited to few millimeters. Finally, image based-approaches [11], [12], should also be highlighted since the determination of the angle of arrival on the array allows to use the same resonator at different positions and thus, increase the coding capacity. However, performance is mainly limited by the directivity of the antenna array which can only be significantly increased by increasing the frequency. Compared to [7], the proposed approach reduces the complexity of the

The authors are with Univ. Grenoble Alpes, Grenoble INP, LCIS, F-26000 Valence, France.

reader and allows identification and sensing. Also, our method requires a single resonator, and increase the read range to 10 m compared to [8]–[10]. Moreover, and contrary to [11], [12], the proposed method can be applied independently of the operating frequency. Finally, for all cited papers, the real impact tag displacement or the beam scanning, which makes the system non LTI, is not established.

The remainder of the paper is organized as follows: Section II presents the analytical model used to describe the linear time-variant sensor. Section III establishes the performance of the sensing, the identification and the read range of the proposed design. Finally, Section IV concludes the paper.

II. Analytical Model

A. Linear Time-Invariant Systems

Chipless tags are LTI systems. As such, they can be fully characterized by their impulse response $h(t)$ or their transfer function $H(f)$ in the time or frequency domain respectively. Also, if a CT is exited by a CW at frequency f_0, the received signal can be written as:

$$y(t) = |H(f_0)| \cos(2\pi f_0 t + \text{Arg}(H(f_0))) \tag{1}$$

which is also an harmonic function at the same frequency f_0 with an attenuation $|H(f_0)|$ and a phase shift $\text{Arg}(H(f_0))$. Finally, we can see that the CT can only backscatter a signal at the same frequency than the one used by the reader. This observation implies important constraints over signal generated by the reader because LTI systems cannot produce frequency components that are not in the input signal. Also, the read range of a tag in real environment is significantly reduced since a CT has exactly the same behavior as any other objects present inside the environment [6].

However, a CT cannot be considered as LTI systems if the tag includes a non linear element or if the response of the tag is not time-invariant. Note also that this modification cannot be done by the tag itself (as in classical RFID) since CTs are strictly passive transponders, and has to be done by an external action such as the rotation of the tag. Thus, the proposed system is in fact more related to a chipless sensor. Note that in this case, the tag is a LTV system and backscatters a modulated signal.

B. Linear Time-Variant Systems

Chipless tags are classically read by sending an electromagnetic wave toward the tag and measuring the backscattered field. The interaction of a wave with a CT is described by its polarization scattering matrix $\mathbf{S}$ which links the scattered electric field vector E^r, to the incident field vector E^i in vertical v and horizontal h polarizations:

$$\begin{bmatrix} E_v^r \\ E_h^r \end{bmatrix} = \begin{bmatrix} S_{vv} & S_{vh} \\ S_{hv} & S_{hh} \end{bmatrix} \cdot \begin{bmatrix} E_v^i \\ E_h^i \end{bmatrix} \tag{2}$$

where each component in the $\mathbf{S}$ matrix is complex and frequency dependent. Note that since CTs are passive and reciprocal, $\mathbf{S}$ is symmetric *i.e.*, $S_{vh} = S_{hv}$. Moreover, (2) is valid for any scatterer.

If we consider a rotation of the tag by an angle θ under normal incidence, the parameters of the $\mathbf{S}$ matrix at θ are linked to the initial ones by the following expression [13]:

$$\mathbf{S}(\theta) = \mathbf{\Omega}^T \cdot \mathbf{S} \cdot \mathbf{\Omega} \tag{3}$$

where ^{T} is the transpose operator and $\mathbf{\Omega}$ is the rotation matrix:

$$\mathbf{\Omega} = \begin{bmatrix} \cos\theta & -\sin\theta \\ \sin\theta & \cos\theta \end{bmatrix} \tag{4}$$

Also the complex envelope of the reflected signal extracted from (3) in vertical co-polarization (vv), horizontal co-polarization (hh) and cross-polarization (vh) of a general scatterer can be respectively expressed as:

$$\begin{cases} S_{vv}^c(\theta) = S_{vv}^c \cos^2\theta + S_{vh}^c \sin 2\theta + S_{hh}^c \sin^2\theta & \text{(5a)} \\ S_{hh}^c(\theta) = S_{vv}^c \sin^2\theta - S_{vh}^c \sin 2\theta + S_{hh}^c \cos^2\theta & \text{(5b)} \\ S_{vh}^c(\theta) = \dfrac{S_{hh}^c - S_{vv}^c}{2} \sin 2\theta + S_{vh}^c \cos 2\theta & \text{(5c)} \end{cases}$$

The following of the demonstration only considers vertical polarization, but same operations can be applied for all polarizations and final results are presented in the end of the subsection. If this scatterer is now rotated at a constant non-zero angular velocity of ω rad/s, then $\theta = 2\pi f_r t$ where $f_r = \omega/2\pi$ is the rotational frequency. The vertical co-polarization can be written as:

$$S_{vv}^c(t) = \frac{S_{vv}^c + S_{hh}^c}{2} + \frac{S_{vv}^c - S_{hh}^c}{2} \cos 4\pi f_r t + S_{vh}^c \sin 4\pi f_r t \tag{6}$$

Applying Fourier transform leads to:

$$S_{vv}^c(f) = \frac{S_{vv}^c + S_{hh}^c}{2}\delta(f) + \frac{S_{vv}^c - S_{hh}^c - 2jS_{vh}^c}{4}\delta(f - 2f_r) + \frac{S_{vv}^c - S_{hh}^c + 2jS_{vh}^c}{4}\delta(f + 2f_r) \tag{7}$$

Unilateral spectrum corresponding to the real signal in all polarizations are finally presented in (8a), (8b) and (8c).

$$\begin{cases} S_{vv}(f) = \dfrac{S_{vv} + S_{hh}}{2}\delta(f - f_0) + \dfrac{S_{vv} - S_{hh} - 2jS_{vh}}{4}\delta(f - f_0 - 2f_r) + \dfrac{S_{vv} - S_{hh} + 2jS_{vh}}{4}\delta(f - f_0 + 2f_r) & \text{(8a)} \\ S_{hh}(f) = \dfrac{S_{vv} + S_{hh}}{2}\delta(f - f_0) + \dfrac{S_{hh} - S_{vv} + 2jS_{vh}}{4}\delta(f - f_0 - 2f_r) + \dfrac{S_{hh} - S_{vv} - 2jS_{vh}}{4}\delta(f - f_0 + 2f_r) & \text{(8b)} \\ S_{vh}(f) = \dfrac{2S_{vh} - j(S_{hh} - S_{vv})}{2}\delta(f - f_0 - 2f_r) + \dfrac{2S_{vh} + j(S_{hh} - S_{vv})}{2}\delta(f - f_0 + 2f_r) & \text{(8c)} \end{cases}$$

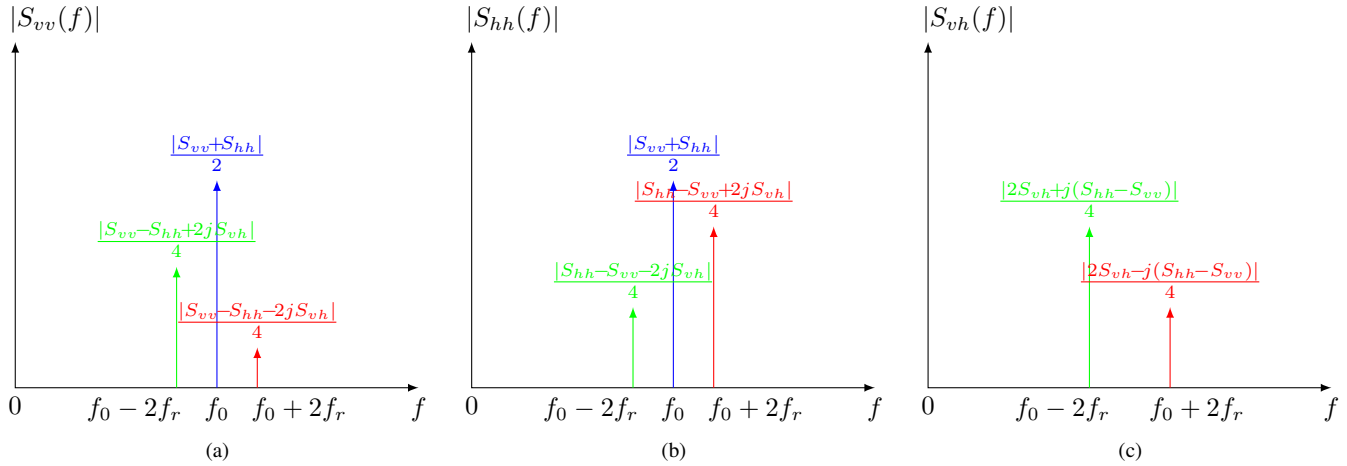

Fig. 2. Unilateral spectrum of a rotating tag at f_r, impinged by a CW at f_0 in (a) vertical co-polarization [see (8a)], (b) horizontal co-polarization [see (8b)] and (c) cross-polarization [see (8c)].

Finally, note that since each scattering point of the tag remains at a constant distance of the antenna, its associated radial velocity is equal to zero. Thus, the described phenomenon is not linked to Doppler or micro-Doppler effect [14].

Fig. 2 presents the spectrum of the three different polarizations in free space environment (and assuming a perfect isolation between the transmitting and receiving path). Vertical and horizontal polarizations are characterized by a spectrum composed of three peaks whereas only two peaks are present in cross-polarization. Each peaks is weighted by a coefficient depending on the scattering matrix and given by (8a), (8b) and (8c). Note that this spectrum is only defined when the tag is rotating; if the tag is motionless, the spectrum is composed of a single peak located at $f = f_0$ of amplitude $S_{vv}(\theta)$, $S_{hh}(\theta)$ or $S_{vh}(\theta)$. Also, side peak positions are function of the angular velocity whereas their amplitudes are function of the polarization scattering parameters. This observation will be used to realize respectively sensing and identification of the CTs. Finally, we will see that the part of the power which is not located at $f = f_0$ allows to drastically increase the read range of these rotating sensors. All these points will be discussed in Section III.

C. Reader Architecture

Since chipless tags are LTI systems, classical reading implies that the reader sends a UWB signal covering all the tag operating frequencies because the tag itself cannot generate a frequency which is different of the ones used by the reader. Thus, all architectures relies on complex UWB designs based in time [5] or frequency [3], [7], [15]. Moreover, since other objects in the environment are also LTI systems, they also reflect power at the same frequencies. Classical procedure to separate the tag from the environment, called empty measurement, is based on the difference between the response of the tag (in the environment) and the environment without the tag. However, the associated residual environment cannot be maintained arbitrary low which considerably limits the performance of the chipless technology [6].

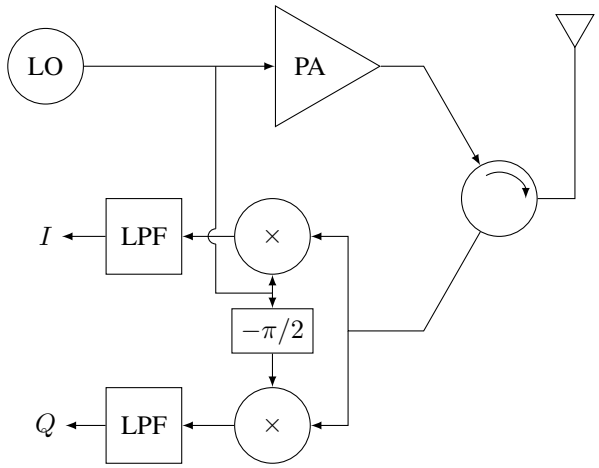

Fig. 3. Architecture of the reader allowing to realize the identification and the sensing of the LTV chipless sensor for a single polarization.

When a tag is rotating (*i.e.*, LTV system), (8a), (8b) and (8c) show that if a single frequency f_0 is used by the reader, the rotated tag is able to generate a power at $f_0 - 2f_r$ and $f_0 + 2f_r$. These two side lobes can be used to realize both sensing and identification of the tag. Also they can be easily detected since the reader does not generate any power in these bands (received power has simply to be compared to the noise floor). Thus, measurement can be realized at a single frequency (*i.e.*, without using any UWB signal). This principle was successfully used in [8]–[10]. The reader architecture is, in this case, totally different compared to classical UWB chipless readers since a simple narrow band reader with an IQ demodulation (or an envelope detector) in the receiving path can be used. In that sense, this architecture is very closed to the one used by classical UHF RFID readers. Fig. 3 presents the architecture of the reader allowing to realize the identification and the sensing of the proposed LTV chipless sensor. Finally and contrary to chipless RFID, since leakage, coupling and/or reflections with objects present inside the environment are LTI systems and reflect a power only at f_0,

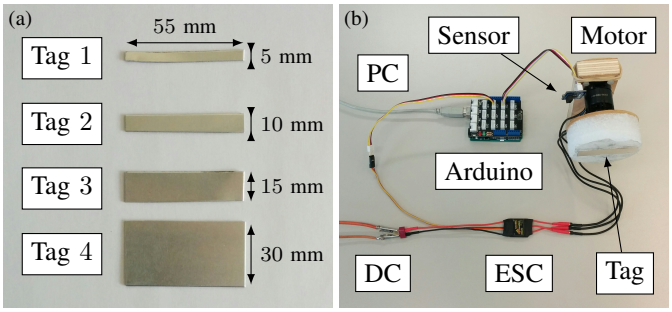

Fig. 4. (a) Chipless tags used to measure the rotational speed. (b) Rotational support used to rotate the tags.

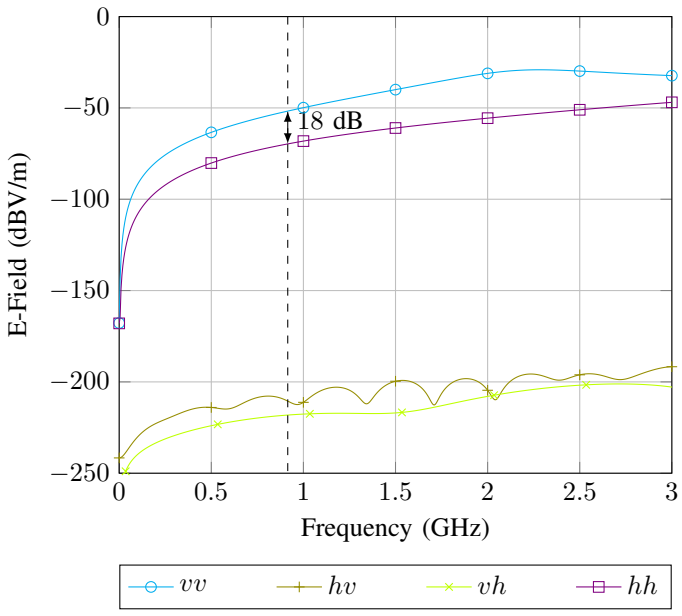

Fig. 5. Simulated backscattered E-Field of a vertical rectangular scatterer of dimension 55×15 mm (Tag 3) for all polarizations.

the signal backscattered by the tag can easily and efficiently be separated from the one associated to the environment, using a simple high pass filter after the demodulation (*i.e.*, without using empty measurement).

III. Results

A. Tag Design and Measurement Bench

Chipless tags investigated in this paper are metallic rectangular scatterers and are presented in Fig. 4(a). Tags have been machined from a 0.8 mm thickness aluminum sheet. All scatterers have the same length of 55 mm, but different widths of $\{5; 10; 15; 30\}$ mm. Fig. 5 presents the backscattered E-field of Tag 3 (55×15 mm) in vertical position for all polarizations using CST Microwave Studio. Tag is impinged with a plane wave and electric field is measured using a farfield probe at a distance of 1 m from the tag. Simulation is performed using the transient solver of CST over a bandwidth of 3 GHz. Note that the E-field in a given polarization is directly proportional to the associated scattering parameter. From the simulated results, we can see that the tag only backscatters in the horizontal (hh)

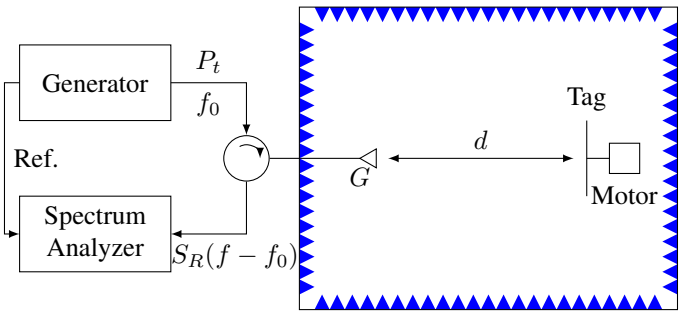

Fig. 6. Measurement bench used to measure the LTV tags in anechoic chamber.

and vertical (vv) co-polarizations (cross-polarization terms are equal to 0 due to the symmetry of the structure). Also, at 915 MHz, the difference between the received E-field in vertical and horizontal co-polarization is higher than 18 dB which shows that the scattering matrix takes the simple form:

$$S_{tag} \approx \begin{bmatrix} S_{vv} & 0 \\ 0 & 0 \end{bmatrix} \tag{9}$$

If we now consider the rotation of this tag at a frequency f_r, impinged by a CW at f_0 in vertical polarization, then (8a) can be used to predict the spectrum of the backscattered signal:

$$S_{vv}(f) = \frac{S_{vv}}{2}\delta(f - f_0) + \frac{S_{vv}}{4}\delta(f - f_0 \pm 2f_r) \tag{10}$$

which corresponds to a simple AM modulation with a modulation index of 1. Note that the two side lobes have exactly the same amplitude and that half of the backscattered power is actually modulated by the rotating tag.

The measurement bench is described in Fig. 6 and is composed of a vector signal generator (Agilent N5182A) and a spectrum analyzer (Tektronix RSA 3408A). Both instruments are connected respectively to the antenna (A.H. Systems, inc. SAS-571) through a circulator. The generator transmits a CW at $f_0 = 915$ MHz with a power of $P_t = 0$ dBm. Also, no modulation is used on the reader side. Spectrum analyzer is used in reception to observe a frequency span of 500 Hz around f_0. The tags have been placed at a distance of 1.5 m of the antennas to fulfill farfield conditions. Note that spectrum analyzer and generator use the same 10 MHz reference signal to achieve phase synchronization between the two instruments. For each measurement, tags are placed on a rotating support which is driven by a brushless motor [see Fig. 4(b)]. Rotational speed is controlled using an Electronic Speed Control (ESC) connected to a micro-controller (Arduino Uno). Also, since exact rotational speed cannot be known from the command sent to the ESC, an external sensor has been added, and connected to the micro-controller, to accurately estimate the rotational speed in real-time.

B. Sensing

Sensing using chipless tags has already been investigated to measure different physical quantities based on frequency shift [16], [17], phase or delay shift [18], amplitude shift [19]–[21] or combination of the previous techniques [22]. Note that

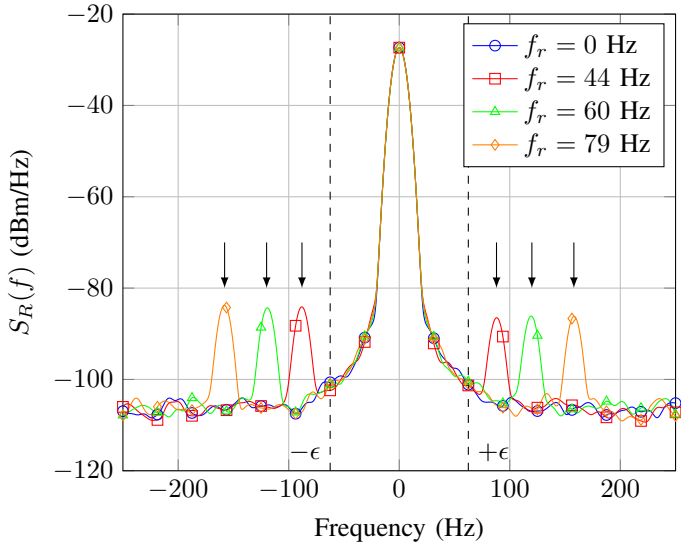

Fig. 7. Power spectral density received for different rotational speed in vertical co-polarization for Tag 3. Sensing is realized based on the frequency position of the side lobes.

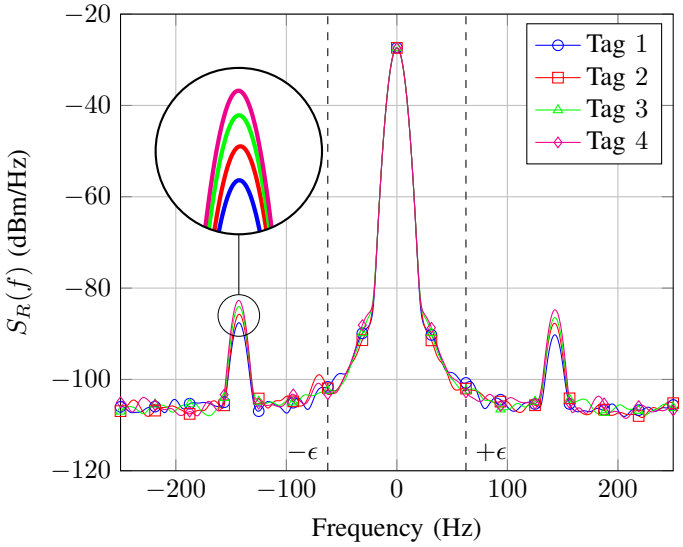

Fig. 8. Power spectral density received for the different tags in vertical co-polarization at a fixed rotational frequency of 58 Hz. Identification is realized based on the amplitude of the side lobes.

sensing can be done based on the impulse response or the transfer function of the tag. However in each case, the sensor is a LTI system.

The proposed sensor is radically different since it corresponds to a LTV system and cannot be described by a impulse response or a transfer function. Instead, the backscattered signal is modulated by the rotation of the tag. Thus, the information associated to the angular velocity is encoded in the frequency position of the backscattered side lobes. Since the backscattered power of the tag is different when the tag is motionless and when the tag is rotating, Fig. 7 presents the received PSD $S_R(f)$ of Tag 3 for $f_r = 0$ and for $f_r \neq 0$. Exact rotational frequency is measured by the external sensor. This scatterer is impinged by a CW wave at a frequency of $f_0 = 915$ MHz. We can see that for a zero speed, the tag backscatters a power only at f_0 (which correspond to 0 Hz after the demodulation done by the spectrum analyzer) since the tag is a LTI system. Note that the amplitude of the peak does not only depend on the tag but also on the leakage of the circulator and the reflection of the others object (since all these perturbations are also LTI systems). On the other side, when the tag is rotating, the presence of the carrier is still visible but two peaks located at $f_0 \pm 2f_r$ appear as expected by the introduced model. Vertical arrows have been added on the curve to indicate theoretical location for each rotational frequency. For example, for a rotational frequency of 44 Hz (measured with the external sensor), the position of the side lobes are located at ± 88 Hz from the central peak. Note that this results is in good agreement with the theory [see (8a)]. Also the amplitude (and phase) of these peaks only depend on the tag since it is the only LTV system in the environment. Finally, one can remark that these two peaks can be easily detected since the noise floor is as low as -110 dBm/Hz (without any empty measurement).

C. Identification

Chipless tags classically encode their information into the peak (or deep) locations along the frequency by using resonant scatterers. This supposes that the tag is impinged with a pulse (or an harmonic sweep) covering all the tag operating bandwidth. The encoding proposed in this paper is very different since the tag is excited by a CW signal. Also note that We introduce an identification method based on the amplitude of the peaks backscattered by the rotating tag. The amplitudes of the peaks depends, as shown by (8a), (8b) and (8c), on the parameters of the polarization scattering matrix. Theses parameters can be controlled by carefully designing the geometry of the chipless sensor (at a single frequency).

Also, note that over non-isolated channels, the amplitude of the peak located at f_0 is also a function of leakage between the two antennas and the reflections of different objects present inside the environment. This power is, in practice, significantly higher than the one backscattered by the tag. Thus, a robust coding scheme cannot be based on the power received at f_0 to identify the tag. To overcome this limitation, an encoding based on the amplitude of the two side lobes is introduced. This method presents a high robustness since the associated power is independent of the leakage or the power reflected by the environment. Fig. 8 presents the PSD of the received signal for the four different tags (see Fig. 4) at the same rotational frequency $f_r = 71$ Hz. Note that these tags have not been designed to resonate at the operating frequency (as it is the case for frequency coded CTs). We can see that the power of the side lobes depends on the shape of the rotating tag and can thus be used to identify the tag for a given configuration.

In order to provide an estimator which can characterize the ability of the rotating tag to backscatter power at frequencies different than the one used by the reader in different (known) configurations, the delta RCS initially introduced in [23], can be used. As shown in [24], side lobes power in the frequency

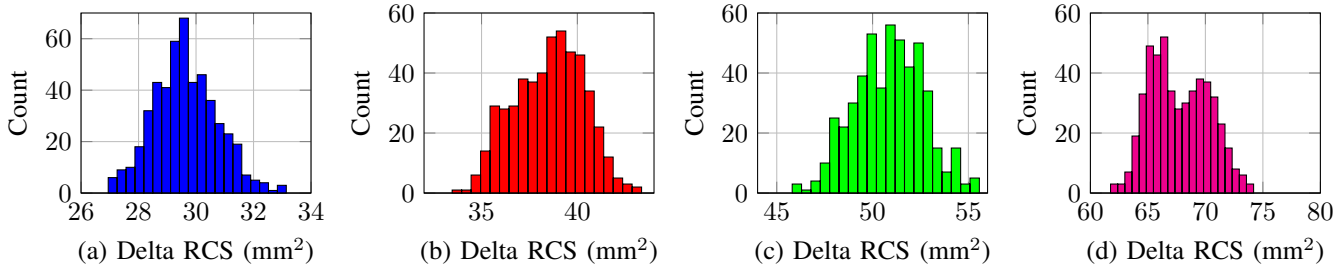

Fig. 9. Histogram of the delta RCS σ_d for the different rotating tags: (a) Tag 1, (b) Tag 2, (c) Tag 3 and (d) Tag 4. Number of measurement is equal to 500 in each case.

domain can be directly linked to the delta RCS σ_d of any modulated tag:

$$\sigma_d = \frac{(4\pi)^3 d^4}{P_t G^2 \lambda^2} \times \left[\int_{f_0-b}^{f_0-\epsilon} S_R(f-f_0)\,\mathrm{d}f + \int_{f_0+\epsilon}^{f_0+b} S_R(f-f_0)\,\mathrm{d}f \right] \quad (11)$$

where d is the distance between the antenna of gain G and the rotating tag (see Fig. 6). Received signal is measured over a span of $2b = 500$ Hz around f_0. Static component is removed over a bandwidth of $2\epsilon = 125$ Hz (see dashed lines in Fig. 8). Also, the term inside the bracket of (11) corresponds to the dynamical power $P_{bs\,d}$ of the backscattered signal. Note that delta RCS obtained from (11) has been introduced for classical UHF tags (which can switch between two different impedance states). However, this frequency definition could be extended to any LTV system. Thus, a rotating tag can be characterized by a delta RCS exactly as a chipped UHF RFID tag. Note that, when the tag is motionless, power associated to side lobes (and delta RCS) is equal to zero. Motionless measurement corresponds a measurement (with the tag) at rotational frequency of 0 Hz. We can remark that delta RCS increases with the surface of the tag. Also repetitions of 500 measurements have been done for each tag and histogram of delta RCS, obtained from (11), is presented in Fig. 9. As a first approximation, the obtained results can be fitted by a Gaussian law. Table I presents the mean value and the standard deviation of the delta RCS of the measured tags. Also, we can see that this measurement bench is characterized by an averaged precision of $3\,\mathrm{std}(\sigma_d) = 4.8$ mm^2. Finally coding capacity of the rotating tags can be estimated from this study. If we consider short-circuited dipole scatterer, maximum RCS is obtained at the resonance frequency and is equal to $\sigma_{max} = \frac{G^2\lambda^2}{\pi} = 920$ cm^2 at 915 MHz [25]. Delta RCS produced during the rotation of this scatterer is lower and equal to $\sigma_{d,\max} = \frac{G^2\lambda^2}{8\pi} = 115$ cm^2. Assuming now that σ_d of a tag can take any value in between $\sigma_{d,\max}$ and 0 cm^2, the number of different tags with a detection rate of 98% can be obtained with $N = \frac{\sigma_{d\,max}}{3\,\mathrm{std}(\sigma_d)}$ and corresponds to a coding capacity of $C = \log_2(N) = 11$ bits. Thus, this metric can be used to identify different tags with a coding capacity of 11 bits in different (known) configurations.

TABLE I
MEAN VALUE AND STANDARD DEVIATION OF DELTA RCS FOR THE DIFFERENT ROTATING TAGS.

	σ_d (dBsm)	σ_d (mm^2)	std(σ_d) (mm^2)
Motionless	−49.98	10.0	0.785
Tag 1	−45.28	29.63	1.104
Tag 2	−44.14	38.52	1.805
Tag 3	−42.94	50.87	1.794
Tag 4	−41.69	67.72	2.575

D. Multiple Tag Reading

Chipless technology does not support multiple tag reading since all tags backscatter a signal over the entire bandwidth used by the reader. Thus, if two tags are present in the environment, responses overlap in frequency and identification is generally not possible. To cope with this problem, one can separate the total bandwidth in N sub-bands and design each tag to encode the information in a single sub-band. However, in this case, tag capacity is also reduced by a factor N since each tag can only encode over a small fraction of the full bandwidth. Some other examples are based on orthogonal separation (in polarization, orientation, direction...) but methods can not be generalized to N tags and the same conclusions apply since in each case chipless tags, are still LTI systems.

On the other side, the proposed design is radically different and offers an efficient way to read multiple tags without scarifying the coding capacity. As long as each sensor is rotating at a different speed, the associated PSD remains orthogonal between each sensors. Thus, the proposed design allows, for the first time, to read N tags with the same coding capacity (*i.e.*, 11 bits, see Section III.C). Configuration and results are presented in Fig. 10 where two rotating tags (Tag 1 and Tag 3) are controlled by separate ESC which allows to select independently the rotational speed for the two motors. Results show that Tag 1 (resp. Tag 3) has a rotational frequency of 29 Hz (resp. 72 Hz) and an amplitude ratio of 4.1 dB which is in very good agreement with the ratio of the tags alone (3.6 dB, see Fig. 8). Thus, it is possible to realize simultaneously sensing (by estimating the peaks position) and identification (by estimating the amplitude value) as long as the two rotational speeds are different. Note that if the rotational speeds are identical, the two responses are superimposed and multiple identification is not possible (as in classical chipless RFID).

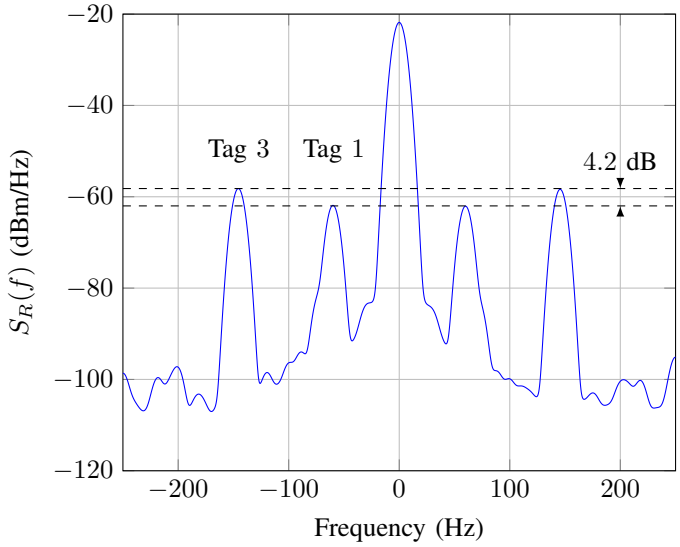

Fig. 10. Multiple tag reading (Tag 1 and Tag 3) at $f_0 = 915$ MHz with a transmitted power of $P_t = 15$ dBm and a distance of $d = 80$ cm in anechoic chamber.

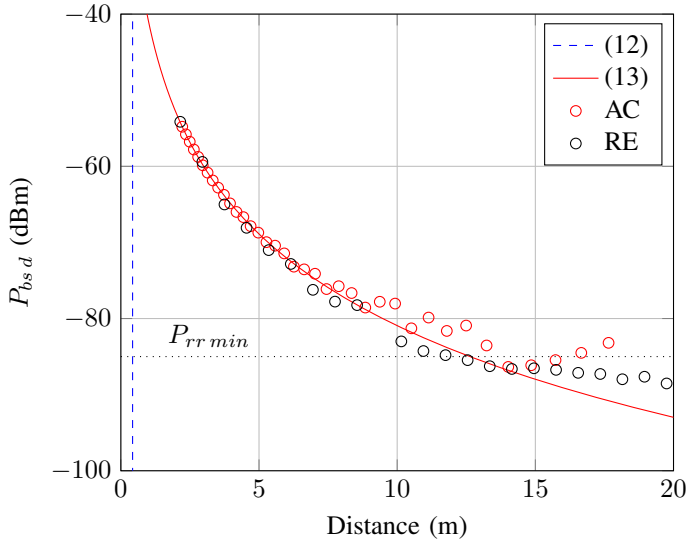

Fig. 11. Modulated power as a function of the equivalent distance over non-isolated channels for Tag 4 ($\sigma_d = 67.72$ mm^2). Dot markers have been obtained from measurement in Anechoic Chamber (AC) and Real Environment (RE).

E. Read Range

Read range in real environments (*i.e.*, non-isolated channels) of classical chipless tags and the proposed tags are radically different. Since CTs are LTI systems, their associated read range, assuming a reading method which compensate the environment using empty measurement, is mainly limited by the level of the residual environment $|\epsilon(f)|^2$ [6]:

$$d_{LTI} \leq \sqrt[4]{\frac{G_t G_r \lambda^2 \sigma(f)}{(4\pi)^3 |\epsilon(f)|^2}} \tag{12}$$

where G_t and G_r are the transmitting and receiving antenna gains, and $\sigma(f)$ the RCS of the CT. Note that this formula does not depend on the transmitted power neither on the reader sensitivity. Finally, the read range is usually lower than 50 cm in real environments.

When the tag is rotating, CT cannot be considered as a LTI system anymore. In this case read range in real environments (*i.e.*, non-isolated channels) could be derived from a modified form of the radar equation [6] and is proportional to the backscattered power which is not located at $f = f_0$. Note that this power is directly linked to the delta RCS σ_d of the tag:

$$d_{LTV} \leq \sqrt[4]{\frac{P_t G_t G_r \lambda^2 \sigma_d}{(4\pi)^3 P_{rr\,min}}} \tag{13}$$

where P_t and $P_{rr\,min} = 2N_0 b$ are the transmitted power and the receiving reader sensitivity respectively (*i.e.*, the minimal differential backscattered power which can be detected by the reader). Finally, we can see with (13) that read range can be increased with the transmitted power and can reach dozens of meters in the ISM bands.

Measurements have been done in anechoic chamber by evaluating the modulated power $P_{bs\,d}$ of Tag 4 as a function of the transmitted power P_t from 13 to -24 dBm in the same configuration (*i.e.*, fixed distance). For each P_t value, the equivalent distance, assuming an effective isotropic radiated power of 4 W is determined. Finally, the modulated power $P_{bs\,d}$ is extracted from $S_R(f)$ and is plotted as a function of the estimated distance. Results are presented in Fig. 11. Bounds obtained from (12) and (13) are also reported. Read range of the non-rotating tag depends on the tag RCS and the residual environment. The RCS value at 915 MHz has been determined by simulation (similar to Fig. 5) and is equal to $\sigma = \sigma_{vv} = -37$ dBsm and the residual environment has been set to $|\epsilon(f)|^2 = -50$ dB. Corresponding read range is equal to 42 cm (independently of the transmitted power). On the other side, when the tag is rotating, read range is extracted from (13) and is equal to 13 m assuming that $P_{rr\,min} = -85$ dBm. Measurements are in good agreement with the theory since the measured modulated power is a decreasing function of the distance (and transmitted power) until $d = 13$ m (which correspond to a $P_{rr\,min} = -85$ dBm) and remains constant for higher distances due to the noise floor of the system present in the bandwidth. Measurements have also been done in outdoor environment with a fixed power $P_t = 36$ dBm and by modifying the distance between the rotating tag and the antenna and provide similar results.

Thus, the rotation of the tag can actually breaks the inherent limitation in read range associated with the chipless technology and reach dozen of meters while satisfying regulation constraints.

IV. Conclusion

The paper presents the first chipless sensor which cannot be considered as a linear time-invariant system. This sensor is able to break the linearity classically associated with the chipless technology due to the rotation of its support. The backscattered signal is then modulated in both time and frequency domains. This technique allows to use the sensor

to accurately estimate its rotational speed and to identify the tag with a simple CW reader. Sensing and identification are realized based on the position and the amplitude of the side lobes of the modulated backscattered signal respectively. Also, multiple tag reading without reducing the coding capacity is also demonstrated for the first time with a chipless sensor. Finally, both identification and sensing can be done at distance higher than 10 m which outperforms classical chipless read range by a factor of 30.

REFERENCES

[1] R. R. Fletcher, "Low-cost electromagnetic tagging: design and implementation," Ph.D. dissertation, Massachusetts Institute of Technology, 2002.

[2] A. Vena, E. Perret, and S. Tedjini, "Chipless RFID tag using hybrid coding technique," *IEEE Trans. Microw. Theory Techn.*, vol. 59, no. 12, pp. 3356–3364, Dec. 2011.

[3] A. Vena, E. Perret, and S. Tedjni, "A depolarizing chipless RFID tag for robust detection and its FCC compliant UWB reading system," *IEEE Trans. Microw. Theory Techn.*, vol. 61, no. 8, pp. 2982–2994, Aug. 2013.

[4] N. Barbot, O. Rance, and E. Perret, "Chipless RFID reading method insensitive to tag orientation," *IEEE Trans. Antennas Propag.*, accepted.

[5] M. Garbati, E. Perret, R. Siragusa, and C. Halope, "Ultrawideband chipless RFID: Reader technology from SFCW to IR-UWB," *Microw. Mag.*, vol. 20, no. 6, pp. 74–88, Jun. 2019.

[6] N. Barbot, O. Rance, and E. Perret, "Classical RFID vs. chipless RFID read range: Is linearity a friend or a foe?" *IEEE Trans. Microw. Theory Techn.*, accepted.

[7] H. El Matbouly, S. Tedjini, K. Zannas, and Y. Duroc, "Chipless sensing system compliant with the standard radio frequency regulations," *IEEE RFID J.*, vol. 3, no. 2, pp. 83–90, Jun. 2019.

[8] C. Herrojo, J. Mata-Contreras, F. Paredes, A. Núñez, E. Ramon, and F. Martín, "Near-field chipless-RFID system with erasable/programmable 40-bit tags inkjet printed on paper substrates," *IEEE Microw. Wireless Compon. Lett.*, vol. 28, no. 3, pp. 272–274, Mar. 2018.

[9] J. Mata-Contreras, C. Herrojo, and F. Martín, "Application of split ring resonator (SRR) loaded transmission lines to the design of angular displacement and velocity sensors for space applications," *IEEE Trans. Microw. Theory Techn.*, vol. 65, no. 11, pp. 4450–4460, Nov. 2017.

[10] C. Herrojo, J. Mata-Contreras, F. Paredes, and F. Martín, "Microwave encoders for chipless RFID and angular velocity sensors based on S-shaped split ring resonators," *IEEE Sensors J.*, vol. 17, no. 15, pp. 4805–4813, Aug. 2017.

[11] M. G. Pettus, "RFID system utilizing parametric reflective technology," U.S. Patent 7 460 014B2, Dec. 2, 2008.

[12] D. H. Nguyen, M. Zomorrodi, and N. C. Karmakar, "Spatial-based chipless RFID system," *IEEE RFID J.*, vol. 3, no. 1, pp. 46–55, Mar. 2019.

[13] E. F. Knott, J. F. Shaeffer, and M. T. Tuley, *Radar cross section*. SciTech Publishing, Inc., 2004.

[14] V. C. Chen, F. Li, S. . Ho, and H. Wechsler, "Micro-Doppler effect in radar: phenomenon, model, and simulation study," *IEEE Trans. Aerosp. Electron. Syst.*, vol. 42, no. 1, pp. 2–21, Jan. 2006.

[15] S. Preradovic, I. Balbin, N. C. Karmakar, and G. F. Swiegers, "Multiresonator-based chipless RFID system for low-cost item tracking," *IEEE Trans. Microw. Theory Techn.*, vol. 57, no. 5, pp. 1411–1419, May 2009.

[16] E. M. Amin, M. S. Bhuiyan, N. C. Karmakar, and B. Winther-Jensen, "Development of a low cost printable chipless RFID humidity sensor," *IEEE Sensors J.*, vol. 14, no. 1, pp. 140–149, Jan. 2014.

[17] Y. Feng, L. Xie, Q. Chen, and L. Zheng, "Low-cost printed chipless RFID humidity sensor tag for intelligent packaging," *IEEE Sensors J.*, vol. 15, no. 6, pp. 3201–3208, Jun. 2015.

[18] S. Shrestha, M. Balachandran, M. Agarwal, V. V. Phoha, and K. Varahramyan, "A chipless RFID sensor system for cyber centric monitoring applications," *IEEE Trans. Microw. Theory Techn.*, vol. 57, no. 5, pp. 1303–1309, May 2009.

[19] D. Girbau, Á. Ramos, A. Lazaro, S. Rima, and R. Villarino, "Passive wireless temperature sensor based on time-coded UWB chipless RFID tags," *IEEE Trans. Microw. Theory Techn.*, vol. 60, no. 11, pp. 3623–3632, Nov. 2012.

[20] A. Vena, L. Sydänheimo, M. M. Tentzeris, and L. Ukkonen, "A fully inkjet-printed wireless and chipless sensor for CO_2 and temperature detection," *IEEE Sensors J.*, vol. 15, no. 1, pp. 89–99, Jan. 2015.

[21] N. Barbot, O. Rance, and E. Perret, "Angle sensor based on chipless RFID tag," *IEEE Antennas Wireless Propag. Lett.*, vol. 19, no. 2, pp. 233–237, Feb. 2020.

[22] ——, "Cross-polarization chipless tag for orientation sensing," in *2019 49th European Microwave Conference (EuMC)*, Utrecht, The Netherlands, Jan. 2021.

[23] P. V. Nikitin, K. V. S. Rao, and R. D. Martinez, "Differential RCS of RFID tag," *Electron. Lett.*, vol. 43, no. 8, pp. 431–432, Apr. 2007.

[24] N. Barbot, O. Rance, and E. Perret, "Differential RCS of modulated tag," *IEEE Trans. Antennas Propag.*, accepted.

[25] R. Harrington, "Electromagnetic scattering by antennas," *IEEE Trans. Antennas Propag.*, vol. 11, no. 5, pp. 595–596, Sep. 1963.

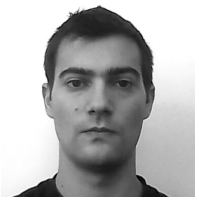

Nicolas Barbot (Member, IEEE) received the M.Sc. degree and Ph.D. degree from the University de Limoges, France. His Ph.D. work in Xlim Laboratory was focused on error-correcting codes for the optical wireless channel. He also realized a post-doctoral work in joint source-channel decoding at L2S Laboratory, in Gif-sur-Yvette, France. Since September 2014, he has been an Assistant Professor at the Université Grenoble Alpes - Grenoble Institute of Technology, in Valence, France. His scientific background at LCIS Laboratory covers wireless communications systems based on backscattering principle which include classical RFID and chipless RFID.

His research interest include transponders which can not be described by linear time-invariant systems. This gathers harmonic transponders which are based on the use of a non-linear component (Schottky diode) or linear time-variant transponders which are based on the modification of their response in the time domain. He also places special interests on antenna design and instrumentation based on these phenomenons.

Etienne Perret (Senior Member, IEEE) received the Eng. Dipl. degree in electrical engineering from the École nationale supérieure d'électrotechnique, d'électronique, d'informatique, d'hydraulique et des télécommunications, Toulouse, France, in 2002, and the M.Sc. and Ph.D. degrees in electrical engineering from the Toulouse Institute of Technology, Toulouse, in 2002 and 2005, respectively.

From 2005 to 2006, he held a post-doctoral position with the Institute of Fundamental Electronics, Orsay, France. In 2006, he was appointed as an Associate Professor of electrical engineering with Grenoble INP Institute of Engineering, Université Grenoble Alpes, Valence, France. From 2014 to 2019, he was a Junior Member with the Institut Universitaire de France, Paris, France, an institution that distinguishes professors for their research excellence, as evidenced by their international recognition. From 2015 to 2020, he was an Appointed Member of the French National Council of Universities. He has authored or coauthored over 200 technical conferences, letters and journal articles, and books and book chapters. He holds several patents. His works have generated about 2800 citations. His current research interests include electromagnetic modeling of passive devices for millimeter and submillimeter-wave applications and wireless communications, especially RFID and chipless RFID, and also include advanced computer-aided design techniques based on the development of an automated codesign synthesis computational approach.